Research on the Corrosion Behavior of X70 Pipeline Steel Under Coupling Effect of AC + DC and Stress

Xinhua Wang, Zuquan Wang, Yingchun Chen, Xuting Song, and Cheng Xu

The coupling effect of stray AC (alternating current) + DC (direct current) and tensile stress-induced X70 pipeline corrosion is complicated with its mechanism uncovered. In this work, the corrosion behavior of X70 pipeline steel under three different corrosion (including an individual AC corrosion, mixed AC + 150 MPa tensile stress corrosion, coupling effect of AC + a 30 A/m^2 DC interference and 150 MPa tensile stress corrosion) conditions in Dagang soil simulated solution was investigated by COMSOL Multiphysics software simulation, electrochemical tests, scanning electron microscope and other techniques. The results indicated that with the increase in AC density, the open-circuit potential of the X70 steel samples was negatively shifted and corrosion rate increased in three different corrosion conditions. The corrosion rates of X70 steel samples under individual AC interference were almost unchanged when 150.9 MPa tensile stress was applied. When applying 30 A/m^2 DC interference, the corrosion rate of X70 steel increases significantly. Therefore, the factors affecting corrosion performance of X70 pipeline steel were DC > AC > stress. Under individual AC interference, uniform corrosion occurred on the X70 steel at an AC current density of less than 30 A/m^2, while the pitting corrosion occurred at an AC current density of greater than 100 A/m^2. The application of tensile stress and DC had a certain inhibitory effect on pitting corrosion.

1. Introduction

In recent years, due to the rapid development of electrified railways and high-voltage transmission lines, there often occurs the parallel/cross-paving between the high-voltage transmission lines and the pipelines. This results in risk for the metallic pipe to suffer from the stray alternating current (AC) and stray direct current (DC)-induced corrosion, and the occurrence of such problem has greatly increased in recent years (Ref 1, 2). Over the past few decades, stray DC has been considered as the greatest impact on the corrosion of buried metallic pipelines. Therefore, many studies have been conducted to understand the mechanism of stray DC-induced corrosion and find ways of protecting the pipelines from stray DC-induced corrosion. The study of AC stray current corrosion lags far behind that of DC stray current due to the ignorance on the effect of stray AC current (Ref 3-6). In recent years, a large number of cases of corrosion failures on buried pipelines caused by stray AC interference have been reported across the world. For example, after laying one X42 pipeline steel coated with fused epoxy powder (FBE) and 500 kV high-voltage AC power transmission wires parallel for one year, it was found that the corrosion rate at the coating damage was as high as 10 mm/a (Ref 7).

When buried pipelines and high-voltage–power transmission lines are laid adjacent to each other, the power transmission lines mainly exert AC coupling effects on the pipelines through electromagnetic induction effects (Ref 8). The corrosion caused by stray AC has begun to be widely concerned by researchers (Ref 9-12). Up to now, there is no universal corrosion mechanism for AC corrosion, and scholars have proposed several theories to study stray AC corrosion. Li et al. (Ref 13) pointed out that the stray AC would induce corrosion on high-strength steel because the steel was in an anodic polarization status in most of the AC circle. It was found that the corrosion potential was shifted negatively by the stray AC. It is related to the ratio of the absolute value of the Tafel slope of the anode to the cathode. Xu and Cheng et al. (Ref 14) found that when the AC current density was between 0 and 400 A/m^2, the corrosion rate increased with the increase in AC current density; the corrosion rate would begin to decline when the AC current density continued to increase to 600 and 800 A/m^2. Mccollum et al. (Ref 15) used "rectifier theory" to explain the reasons why AC interference accelerates metal corrosion. He believes that the anodic and cathodic polarization are not equal, resulting in a net Faraday current, which in turn promotes the corrosion of metals. Goidanich et al. (Ref 16) suggested that if the electrochemical process at the interface between iron and the electric double layer was not completely reversible, the rectification effect of Faraday's Law was not able to explain the stray AC corrosion. In recent years, Wang et al. (Ref 17-19) conducted many studies on the corrosion behavior of X-series pipeline steel under the effect of stray current and discussed the stray current-induced corrosion mechanism of X-series (X65, X70 and X80) pipelines. Also, during the service of pipelines, the CP current could fluctuate due to a number of reasons, such as noncyclic continuous current pulses and AC stray current interference. Liu et al. (Ref 20) studied that the square wave polarization (SWP) technique and slow strain rate tensile test

Xinhua Wang, Zuquan Wang, Yingchun Chen, Xuting Song, and Cheng Xu, Beijing University of Technology, 100 Ping Le Yuan, Chaoyang District, Beijing 100124, China. Contact e-mail: ychen08089@163.com.

were combined to investigate the influence of cathodic potential fluctuation. It was found that the nonstable cathodic polarization accelerated both the anodic dissolution and the cathodic hydrogen evolution.

High-strength pipeline steel is now widely used in the construction of the pipelines as long distance, and high pressure is a necessity for the oil and gas pipelines. The pipeline would inevitably suffer from stress applied by the conveying high-pressure medium, which has an important influence on the thermodynamics and kinetics of high-strength steel pipelines corrosion (Ref 21, 22). With the frequent accidents, the phenomenon of accelerated stress corrosion has drawn more and more attentions. There are some researches on stress corrosion acceleration.

Boven et al. (Ref 23) found that both residual stress and applied stress can accelerate the corrosion behavior of near-neutral NS_4 simulation solution of X65 pipeline steel and promote the formation of corrosion pits and accelerate the corrosion rate. Wei et al. (Ref 24) studied the effect of external tensile stress on pitting behavior of X80 pipeline steel in $NaHCO_3$ + NaCl by electrochemical noise test and potentiodynamic polarization method. The results show that the smaller tensile stress (σ < 100 MPa) can inhibit the pitting corrosion of X80 steel in alkaline soil and the inhibition increases with the increase in stress. However, the occurrence of pitting plays a catalytic role under a larger tensile stress (σ > 200 MPa). Liu et al. (Ref 25) studied that in electrochemical state conversion model for occurrence of pitting corrosion on a cathodically polarized carbon steel in a near-neutral pH solution, the CP fluctuation could occur during service, which would introduce the polarization fluctuation on the steel, resulting in pitting corrosion.

At present, the studies conducted on alternating and direct stray current corrosions do not consider the coupling effect of various factors. In addition, for a pipeline under actual operational conditions, it will be stressed by the conveying medium and also affected by both the alternating and direct stray currents. Till now, the research on corrosion hazards of buried metallic pipelines under the interference of AC and mixed current is still scarce, and that the corrosion mechanism, corrosion behavior and electrochemical protection technology are not still unknown. Thus, the research done in this paper would be of great theoretical and practical value.

2. Experimental

2.1 Experimental Materials and Solutions

X70 high-strength pipeline steel was selected as the experimental material, which mainly composed of irregular acicular body (the chemical composition shown in Table 1). In order to ensure that the main force direction of the sample is the same as the actual stress direction of the pipeline, wire cutting must be carried out along the pipeline radial direction. Size of the sample is as shown in Fig. 1.

The tensile strength of X70 pipeline steel sample is 610 MPa, while the yield strength is 503 MPa at 25 °C. 30% yield strength (Ts = 610 × 30% = 150.9 MPa) was applied to the sample as the experimental tensile stress. The stress of sample was analyzed by COMSOL Multiphysics. Distribution of the stress on the sample surface is shown in Fig. 2 and 3.

According to Fig. 2 and 3, the stress at the narrowest part of the specimen is obviously higher than that of the other parts, and the stress at the narrowest part of the specimen and the fillet transition zone is the largest. Therefore, selecting the center of the sample as the experimental work surface is reasonable. (The working area is 1.8 cm^2.) The sample surface was polished by SiC60 #, 200 #, 400 #, 600 # sandpaper successively and then thoroughly cleaned with ethanol and acetone. The nonworking surface of the sample was coated with silica gel, which has an excellent water resistance. Finally, the sample was placed in a dry box.

The electrochemical tests were operated in Dagang simulated soil solution, which is a typical weak alkaline soil environment (pH = 8.3). The chemical composition to configure Dagang simulated soil solution is given in Table 2 according to the data achieved from the National Natural Corrosion Environmental Test Station.

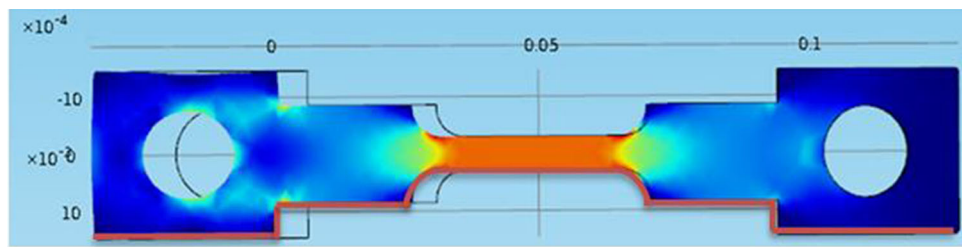**Table 1 Chemical composition of X70 pipeline steel (wt.%)**

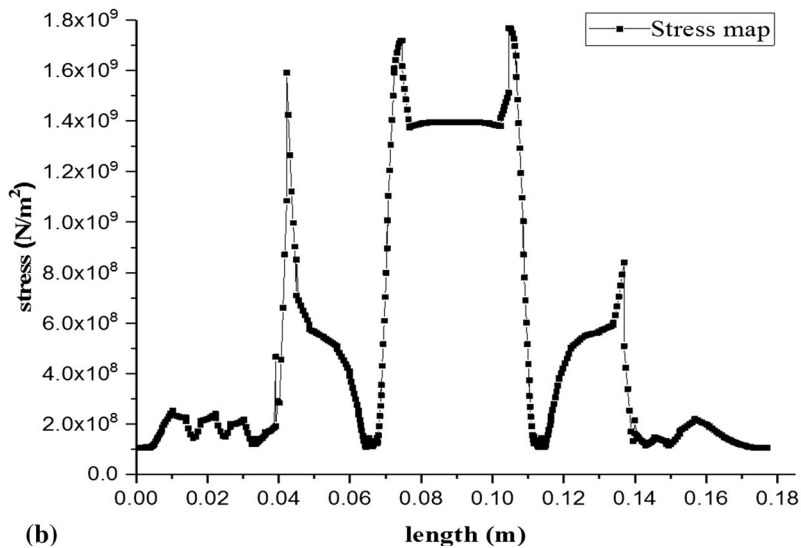| Si	Mn	S	P	C	Fe
0.24	1.48	0.001	0.017	0.045	Balance
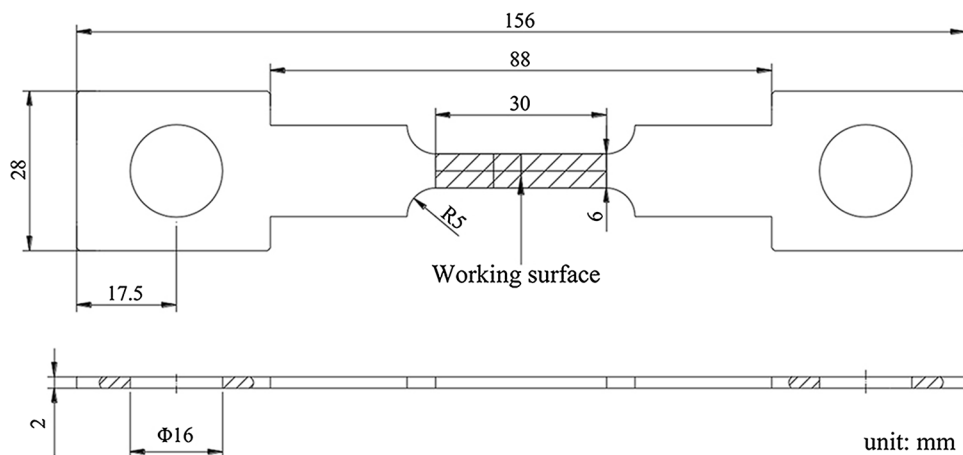
Fig. 1 Schematic and size of the X70 steel sample
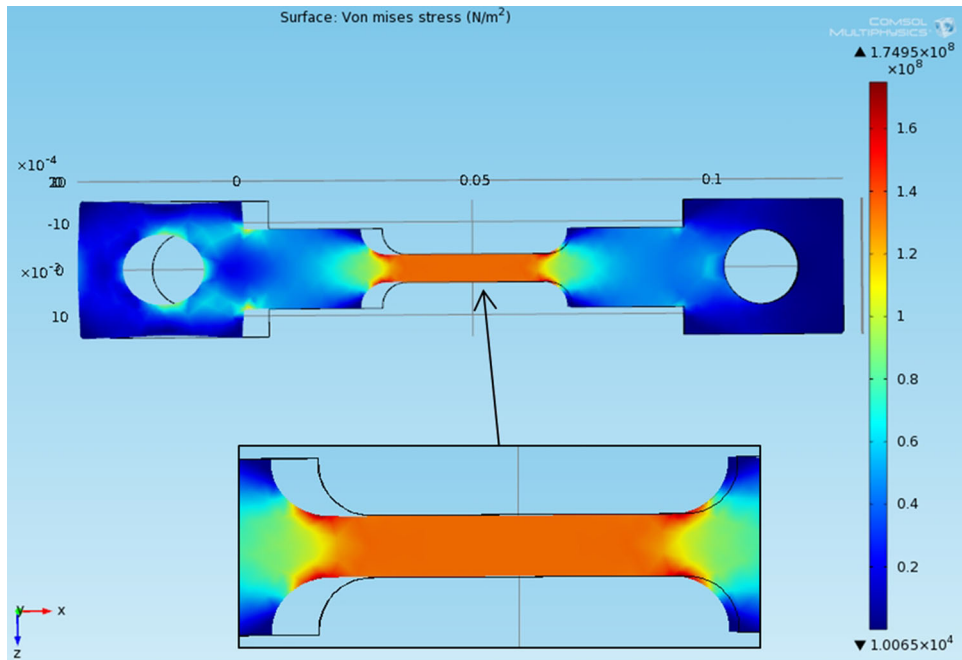
Fig. 2 Simulation of stress distribution of X70 pipeline steel specimen

(a)

(b)

Fig. 3 Stress distribution map (b) along the lower edge (a) of the X70 steel specimen

2.2 Electrochemical Test

Electrochemical testing system, stray current and stress loading device are shown in Fig. 4. The slow tensile tester

(RGM 6050) was used to provide the tensile stress required for the experiment; AC signal generator (SG1005) was used to provide AC signal; constant voltage adjustable DC power supply (KXN-305D) was used to provide DC anode signal;

capacitor C (500uF) was used to prevent direct current from interfering with the AC circuit.; inductance L (15H) was used to prevent the AC from interrupting the DC circuit; this ensures that the two circuits are independent of each other. Princeton's PARSTAT2273 (Princeton, NJ, USA) electrochemical workstation was used to test the open-circuit potential and the polarization curves of X70 steel under the AC + DC + Stress interference. A three-electrode system was used, in which the X70 high-strength pipeline steel sample was used as the working electrode (WE). In addition, the platinum plate was used as the counter electrode (CE), while the saturated calomel electrode (SCE) was used as the reference electrode (RE).

In the AC corrosion experiments, the switch S1 was turned off and the switch S2 was turn on. In the AC circuit, an AC signal generator (SG1005) was used to apply alternating current with different current densities (0, 30, 100, 200, 300 A/m^2) at a frequency of 50 Hz, the current intensity was measured by using an AC meter.

In the AC + Stress corrosion experiments, a 150.9 MPa tensile stress was applied by the slow stress tester (RGM-6050).

The other experimental steps were the same as AC corrosion experiments.

In the AC + DC + Stress corrosion experiments, both the switch S1 and S2 were turn on. In the DC circuit, a DC signal generator (KXN-305D) was used to apply constant DC (30 A/m^2) interference; the current intensity was measured by a DC meter. In the AC circuit, an AC signal generator (SG1005) was used to apply alternating current with different current densities (0, 30, 100, 200, 300 A/m^2) at a frequency of 50 Hz; the current intensity was measured by using an AC meter. Meanwhile, a 150.9 MPa tensile stress was applied by the RGM-6050 slow stress tester.
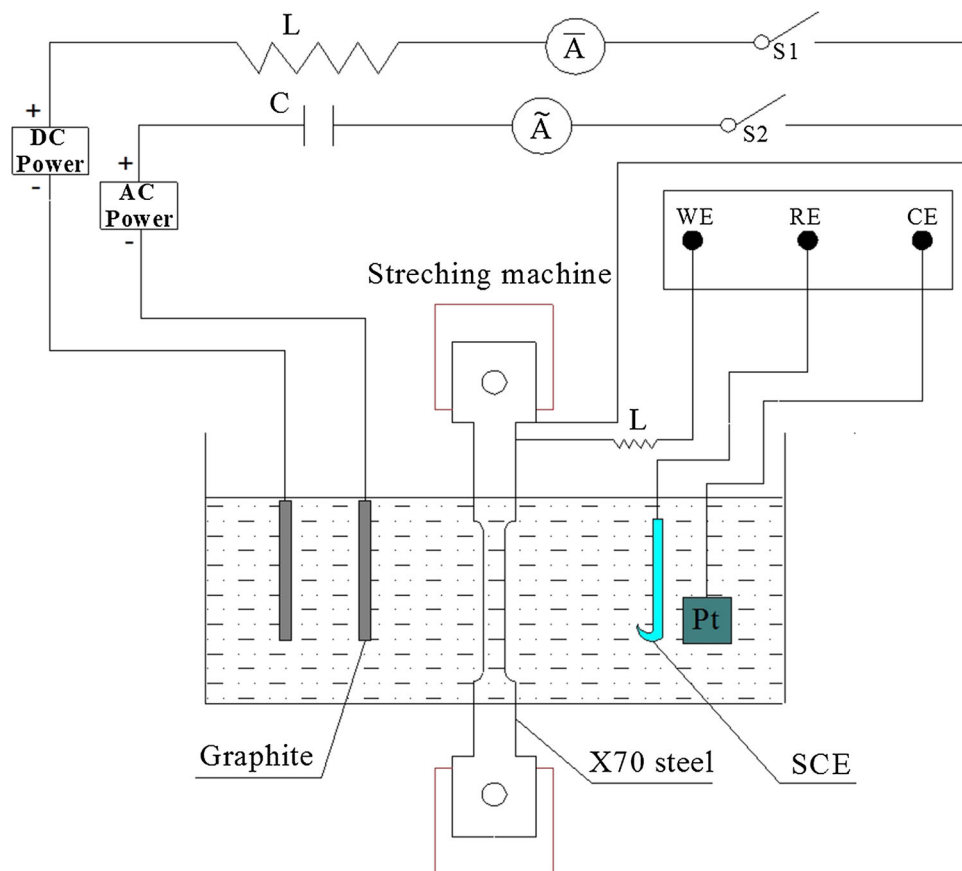
At all three condition experiments, with the application of AC/AC + Stress/AC + DC + Stress interference, open-circuit potential (OCP) and polarization curve were measured after immersing 24 h, after the OCP reached a relatively stable state (0.5 h). The potential polarization curve was tested at a scan rate of 1 mV/s, scan potential range from − 0.6 (versus OCP) to 0.2 V (SCE). In this study, all stray current densities were calculated based on the bare metal area.

2.3 Corrosion Morphology and Corrosion Rate Calculation

The corrosion rate was calculated by weight loss method, and the corrosion electrochemical equivalent was calculated by Eq 1. After the experiment, a digital camera (Canon Kiss X5) was used to photograph the macro-morphology of the corrosion, and then, the corrosive product on the sample surface was removed by using Clark's solution (0.5 g Sb_2O_3 + 1.5 g

Table 2 Chemical composition of Dagang simulated soil solution (g/L)

CaCl$_2$	NaCl	MgSO$_4$·7H$_2$O	KNO$_3$	NaHCO$_3$
1.049	25.020	5.228	0.306	0.249

Fig. 4 Electrochemical test and AC + DC + stress interference experimental device
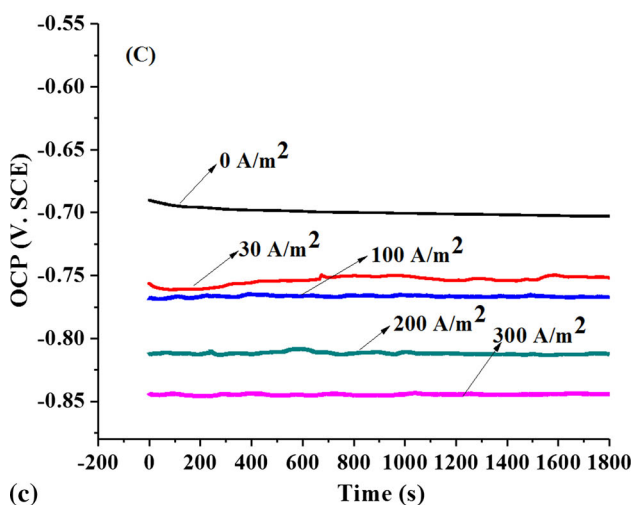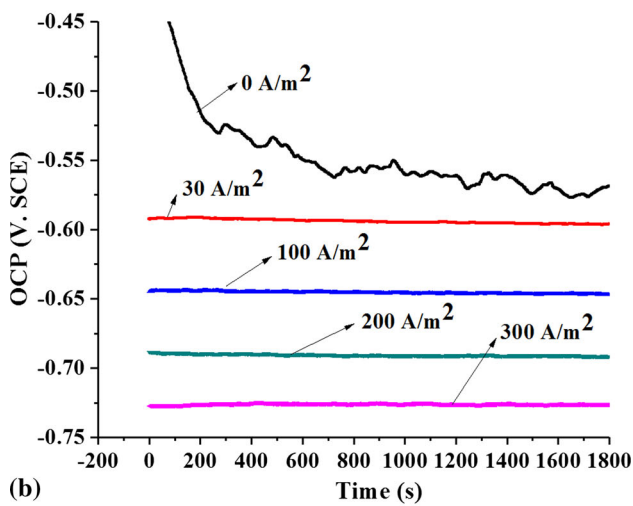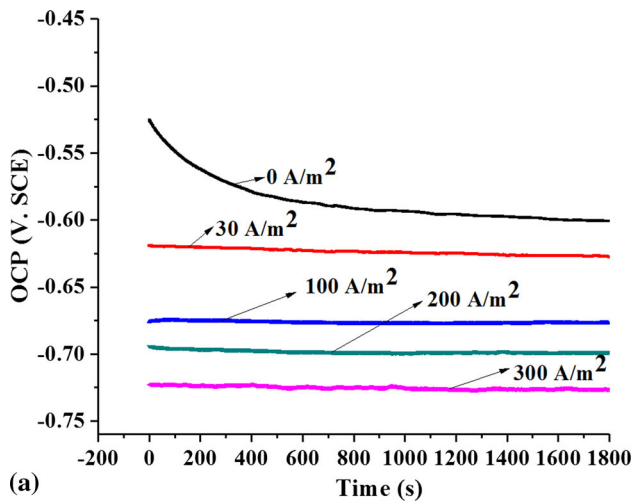
Fig. 5 OCP curve of X70 steel at different AC current densities in (a) Dagang simulated soil solution, (b) Dagang simulated soil solution with 150.9 MPa tensile stress, (c) Dagang simulated soil solution with 150 MPa tensile stress and 30 A/m² DC interference

SnCl$_2$·2H$_2$O + 25 ml HCl) and rinsed with deionized water and acetone. The sample was weighed by a precision electronic balance weighing (Shanghai Nuoke Instruments FA2004B) when it was fully dried. Subsequently, the surface morphology of the sample was observed by a scanning electron microscope (S-3400, Hitachi, Tokyo, Japan)

$$\Delta W = W_0 - W_1, \quad V_{corr} = \Delta W / St \qquad \text{(Eq 1)}$$

where ΔW = average weight loss of the sample, g; W_0 = original weight of the sample, g; W_1 = mass of the sample after removal of the corrosion product, g; S = exposed area of the sample, m²; t = corrosion action time, h; V_{corr} = the average corrosion rate, mm/a.

3. Results and Discussion

3.1 OCP Results of X70 Samples at Various AC Current Densities

The self-corrosion potential, also known as OCP, is a measure of the thermodynamic tendency of a metal to corrode, and the more negative the potential, the more likely the metal is to corrode (Ref [26]).

Figure 5 shows the OCP curve of X70 steel at different AC densities in Dagang soil simulated solution. Firstly, the application of alternating current caused the fluctuation of the OCP curve. It can be considered that AC caused the OCP fluctuation. Second, it can be seen that the OCP shows a negative shift as the AC stray current density increases.

In AC corrosion process, the OCP value shifted from − 0.572 V at no AC interference to − 0.596 V when 30 A/m² AC interference was applied, while the OCP value eventually shifted − 0.726 V when 300 A/m² AC interference was applied. In AC + Stress (150.9 MPa) coupling corrosion process, the OCP value shifted from − 0.582 V at no AC interference to − 0.615 V when 30 A/m² AC interference was applied, while the OCP value eventually shifted − 0.725 V when 300 A/m² AC interference was applied. In the AC + DC (30 A/m²) + Stress (150.9 MPa) coupling corrosion process, the OCP value shifted from − 0.702 V at no AC interference to − 0.753 V when 30 A/m² AC interference was applied, while the OCP value eventually shifted − 0.859 V when 300 A/m² AC interference was applied. This has a good agreement with other researchers (Ref [27]).

Based on the analysis of the data, we can see that the OCP of X70 steel under the coupling of AC + Stress is not different from the OCP under the single AC interference, which indicates that the stress on X70 steel during the elastic phase corrosion performance has little effect. Xu and Cheng et al. (Ref [28]) considered that the static elastic stress exerted on the pipeline steel has a limited influence on its corrosion, while when plastic strain is applied, the pores of the pipeline steel will increase and the activity of apparel will be enhanced.

The OCP of X70 steel, when affected by the coupling of AC + DC + Stress, is smaller than the OCP of single AC interference, indicating that the influence of DC is much more than that of stress. The addition of DC makes the corrosion resistance of X70 steel significantly reduce.

3.2 Polarization Curve Analysis

Figure 6 shows the polarization curves of X70 steel at different AC densities in Dagang solution. At all three conditions, stray current made the X70 steel in active dissolution state without passivation phenomenon. With the increase in AC current density, the corrosion potential of X70 steel moved in a negative direction and the offset of corrosion potential increased with the increase in AC current density.

The kinetic parameters in Tables 3, 4 and 5 are obtained by fitting the polarization curves in Fig. 6, including the corrosion potential E_{corr}, Tafel slopes (anode b_a and cathode b_c), and the fitting is performed according to the literature (Ref 29-31).

The AC has an influence on the anode curve and the cathode curve of Tafel. As the AC current density increases, the slope of the polarization curve of the anode and the cathode becomes more vertical, which indicates the increase in corrosion rate. Compared with the data in Tables 3 and 4, it can be seen that the addition of stress has little effect on the polarization curves of the anodic and cathodic layers, indicating that the affect of stray current on the corrosion rate of X70 steel is more significant than that of stress within the range of elastic deformation; Compared with the data in Tables 4 and 5, it can be found that under the same AC current density and stress condition, the addition of DC makes the slope of the positive and negative polarization curves more vertical, indicating that the DC has more effect on the corrosion rate of X70 steel than the stress.

Bertocci et al. (Ref 32-35) proposed a mathematical model (Eq 2) to explain the polarization behavior of the electrode after applying AC interference by using the theory of electrode reaction kinetics under activation control

$$E_{corr,AC} = E_{corr} - \left(\frac{b_a}{\frac{b_a}{b_c}-1}\right) In \left[\frac{\sum_{k=1}^{\infty}\frac{1}{(k!)^2}\left(\frac{E_p}{2b_c}\right)^{2k}+1}{\sum_{k=1}^{\infty}\frac{1}{(k!)^2}\left(\frac{E_p}{2b_a}\right)^{2k}+1}\right] \quad (Eq\ 2)$$

where $E_{corr,\ AC}$ = corrosive potential with AC interference; E_{corr} = no AC potential interference corrosion; b_a= anode Tafel slope; b_c= cathode Tafel slope; E_p= applied AC peak potential; k = integer

Within Eq 2, $E_{corr,\ AC}$ is a function of b_a/b_c and E_p. The $E_{corr,\ AC}$ shifts when E_p increases, while the direction of its offset depends on b_a/b_c. The $E_{corr,\ AC}$ shifts in the negative direction when $b_a/b_c < 1$, whereas the $E_{corr,\ AC}$ shifts in the positive direction when $b_a/b_c > 1$; when b_a/b_c= 1, the corrosion potential will not shift.

During the experiment, the working area of the sample remained unchanged. The AC current density was proportional to the AC peak potential (E_p). This explains why the corrosion potential of X70 steel shifted negatively with the increase in AC current density.

The experimental conclusion is consistent with Eq 2; the AC interference changes the corrosion potential of X70 steel and shifts the corrosion potential from negative to negative. From the thermodynamic point of view, when the potential becomes negative, it is favorable for the oxidation reaction of iron; X70 steel is more susceptible to corrode.
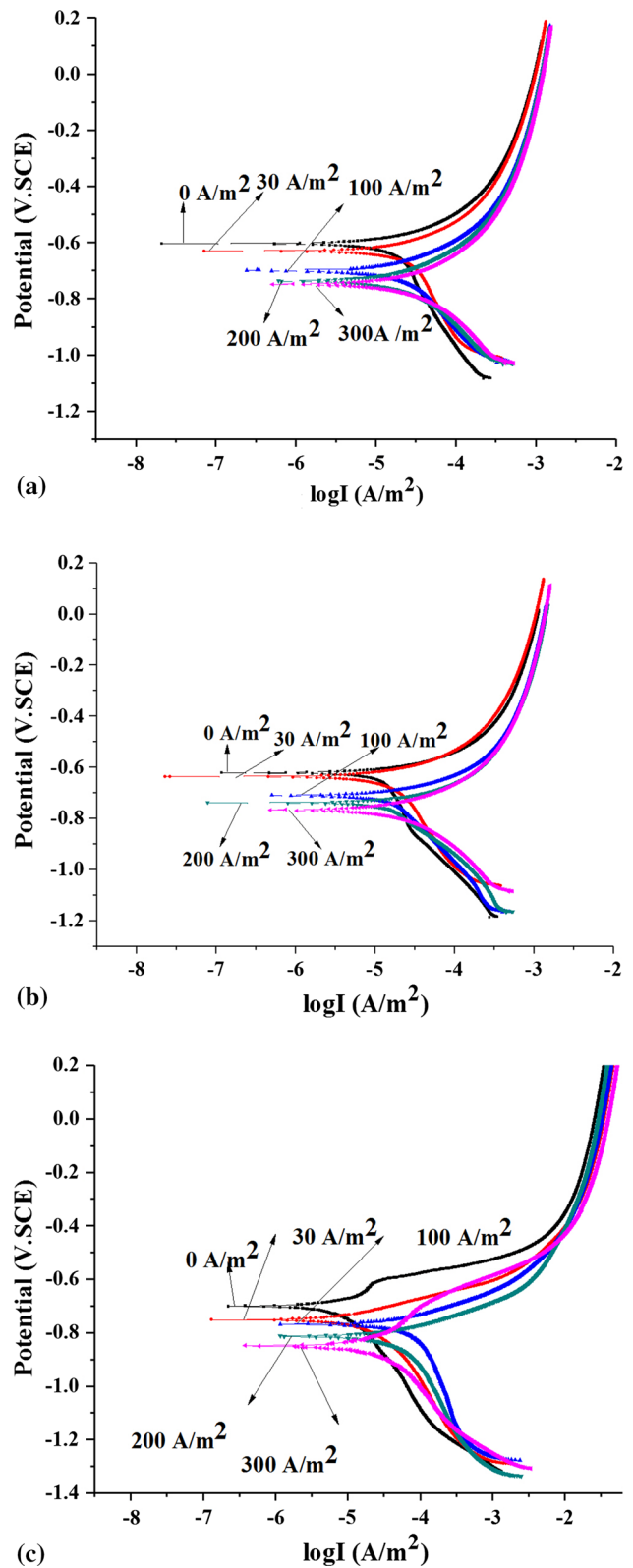

Fig. 6 Polarization curve of X70 steel at different AC current densities in (a) Dagang simulated soil solution, (b) Dagang simulated soil solution with 150.9 MPa tensile stress, (c) Dagang simulated soil solution with 150 MPa tensile stress and 30 A/m^2 DC interference

Table 3   Electrochemical parameters of X70 samples at various AC current densities in Dagang simulated soil solutions

i, A/m^2	E_{corr}, mV, SCE	b_a	b_c	b_a/b_c
0	− 0.604	120.13	924.08	0.13
30	− 0.631	145.66	331.05	0.44
100	− 0.699	178.93	380.70	0.47
200	− 0.736	286.36	485.36	0.59
300	− 0.749	294.04	381.87	0.77

Table 4   Electrochemical parameters of X70 samples at various AC current densities with 150.9 MPa tensile stress application in Dagang simulated soil solutions

i, A/m^2	E_{corr}, mV, SCE	b_a	b_c	b_a/b_c
0	− 0.621	142.41	593.38	0.24
30	− 0.690	156.32	274.25	0.57
100	− 0.709	197.04	298.55	0.66
200	− 0.738	244.59	344.49	0.71
300	− 0.767	289.03	352.47	0.82

Table 5   Electrochemical parameters of X70 samples at various AC current densities with 150.9 MPa tensile stress and 30 A/m^2 DC interference application in Dagang simulated soil solutions

i, A/m^2	E_{corr}, mV, SCE	b_a	b_c	b_a/b_c
0	− 0.702	110.36	735.73	0.15
30	− 0.752	176.34	419.86	0.42
100	− 0.767	198.30	305.08	0.65
200	− 0.812	284.73	360.42	0.79
300	− 0.848	379.06	467.97	0.81

3.3 Corrosion Rate Calculation

The corrosion rate was calculated by weight loss method, and the corrosion electrochemical equivalent was calculated by Eq 1. The average corrosion rate is shown in Fig. 7. In all the three conditions, the corrosion rate is gradually increased when the current density increases. Obviously, the corrosion rate of X70 steel under the coupling of AC + stress is almost the same as the corrosion rate under the single AC. This shows that in the elastic phase, the effect of stress has little effect on the corrosion resistance of X70 steel. Wang et al. (Ref 36) considered that the application of static elastic stress to pipeline steel had a limited effect on its corrosion, but when the applied stress exceeded the yield limit of steel and caused plastic strain, the corrosion rate would change abruptly. As can be seen from Fig. 7, the maximum corrosion rate of X70 steel is 2.5 g/(m^2 h), which occurs when under the coupling of 300 A/m^2 AC + 30 A/m^2 DC + 150.9 MPa stress. The corrosion rate of X70 steel under the interference of 300 A/m^2 AC + 150.9 MPa stress is 0.8 g/(m^2 h). Thus, it can be seen that there is a difference of about 3.1 times in the corrosion rates. The effect of the coupling of AC + DC + Stress is much more serious than
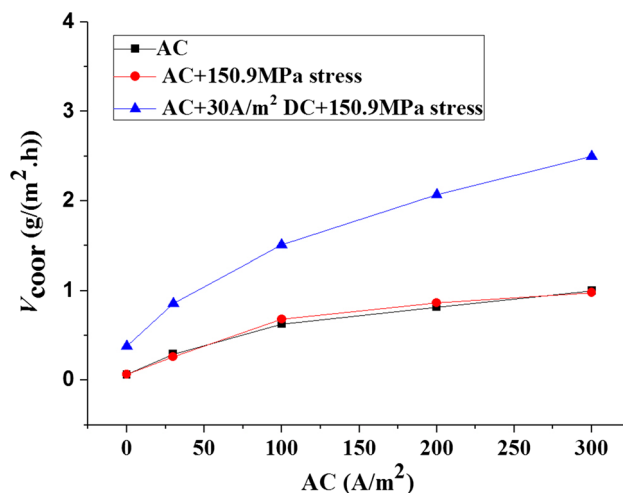
Fig. 7 Comparison of corrosion rate of X70 steel in Dagang simulated soil solution under different experimental conditions

the single-type stray current. The addition of DC interference accelerates the corrosion of the X70.

In the process of DC corrosion, the corrosion rate increases with the increase in the current density, following Faraday's law of electrolysis (Ref 37). The amount of corrosion is proportional to the current density, and thus approximately conforms to the linear rule. AC corrosion is more complex than DC corrosion. There are many mechanisms for corrosion, such as Faraday rectification (Ref 15) and irreversible anode reaction (Ref 16). Because the corrosion process of AC only produces some Faraday current, and the corrosion process of DC completely follows the law of Faraday electrolysis, the influence of DC interference on the corrosion of buried steel pipeline under the same current density is greater.

As can be seen from Fig. 7, in the AC corrosion experiments, in AC corrosion, the corrosion rate increases with the exchange density showing a power function relationship. Wen et al. (Ref 37) experimentally studied on stray current corrosion of coated pipeline steel; he pointed that the relationship between the pit number or pit area and AC current density followed the power function, $y = ai^b$. Our experimental results are in good agreement with that of Wen (Ref 37).

3.4 Corrosion Mechanism Analysis

Scholars have put forward a variety of explanations for AC stray current corrosion. The schematic diagram proposed by Buchler et al. (Ref 38) is more accepted by this subject. Based on that model, this article makes further amendments to make it more in line with electrochemical process rules of AC + DC coupling. When using that model, Buchler divided AC interference into positive and negative half cycles and then analyzed their effects on metal corrosion. In electrochemistry corrosion, the electrode is anodically polarized when the applied current is higher than the equilibrium potential E_0 of the electrode, and the electrode is cathodically polarized when the applied current is lower than the equilibrium potential E_0 of the electrode, where E_0 is the open-circuit potential OCP test result or the corrosion potential $E_{corr, AC}$. Therefore, the AC should be divided into anodic polarization phase and cathodic polarization phase. The anodic polarization stage is the stage where the AC potential is higher than the corrosion potential (the area
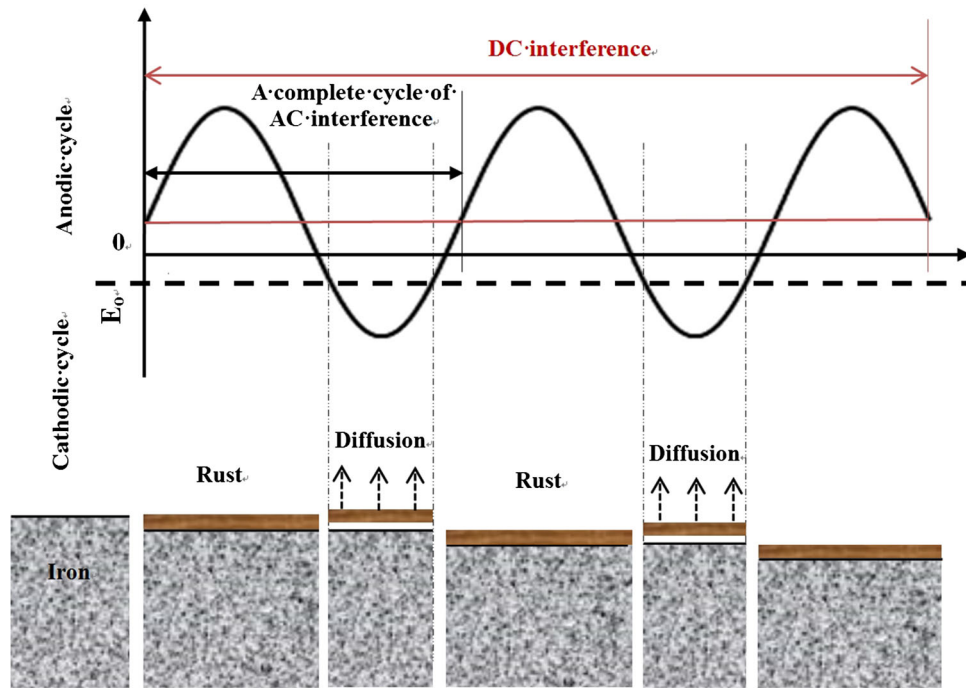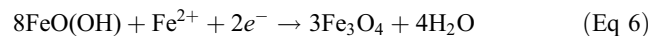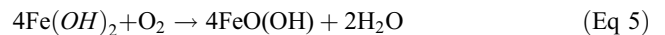
Fig. 8 AC + DC stray current coupling corrosion diagram

above E_0 in Fig. 8). Similarly, the cathodic polarization stage is the stage where the AC stray current potential is lower than the corrosion potential (the area below E_0 in Fig. 8).

As can be seen from Fig. 8, during a complete AC sinusoidal signal cycle, the metal sample is in the anodic polarization for more time than in the cathodic polarization. During the anodic polarization, the metal sample was anodically dissolved and would release Fe^{2+}, and the anodic polarization of iron was irreversible. During the cathode reaction, OH^- was formed on the surface of the sample (Diffusion), and the cathode reaction product combined with the anode reaction product formed a corrosion product film (Rust). In the DC corrosion process, the anode region is a pole where DC flows from the sample surface, in which it occurs to the continuous anodic dissolution of iron. When DC is coupled to AC, during a complete AC sinusoidal signal cycle, the anodic polarization time increases and the cathodic polarization time decreases, so that the anodic reaction on the sample surface becomes the dominant factor, resulting in a net anode current, which made the corrosion reaction of the metal sample accelerated at the chemical reaction kinetic level and the corrosion aggravated.

3.5 Corrosion Morphology Analysis

At all three conditions, it can be seen from the corrosion morphology that the corrosion products are divided into two layers, and the inner layer of the corrosion products, which is near the metal, mainly consist of black products. While the outer layer of corrosion products mainly composed of reddish-brown and brownish-yellow products. Under the action of the alternating current, the corrosion products of X70 steel are mainly composed of $Fe(OH)_2$, $FeO(OH)$ and Fe_3O_4 (Ref 39). The accumulation process for X70 steel surface corrosion product is as shown in Eq 4, 5 and 6.

$$Fe^{2+} + 2OH^- \rightarrow Fe(OH)_2 \qquad \text{(Eq 4)}$$

$$4Fe(OH)_2 + O_2 \rightarrow 4FeO(OH) + 2H_2O \qquad \text{(Eq 5)}$$

$$8FeO(OH) + Fe^{2+} + 2e^- \rightarrow 3Fe_3O_4 + 4H_2O \qquad \text{(Eq 6)}$$

With the increase in AC density, the corrosion degree of X70 steel is more and more serious, the corrosion products increase obviously, and the turbidity of the solution increases. It can be found during the process of rust, the inner black material becomes more and more dense with the increase in alternating current density and is difficult to be removed with a cotton swab (Fig. 9).

The corrosion morphology of X70 steel under AC + Stress coupling is similar to the one under single AC. When the AC density is less than 30 A/m², the corrosion degree of X70 steel is slight, and the corrosion products of outer yellowish brown and reddish brown are less. At the high AC density of 200-300 A/m², the outer layers of yellowish-brown and reddish-brown substances increased and distributed on the experimental surface of the whole sample.

In the AC + DC + Stress coupling corrosion experiments, when 150.9 MPa tensile stress and 30 A/m² DC stray interference are applied, it can be seen that the corrosion products on X70 steel surface obviously increase, indicating that the addition of direct current increases the corrosion of X70 steel.

Figure 10 shows the micro-topography of X70 steel with the removal of corrosion products in Dagang solution under different AC densities. As can be seen from the figure, with the increasing AC density, X70 steel surface becomes more and more rough, the original bright smooth surface of the substrate is corroded in Dagang soil simulation solution. X70 steel surface is relatively smooth under no AC or low AC current density interference ($\leq$ 30 A/m²), also, there is no obvious
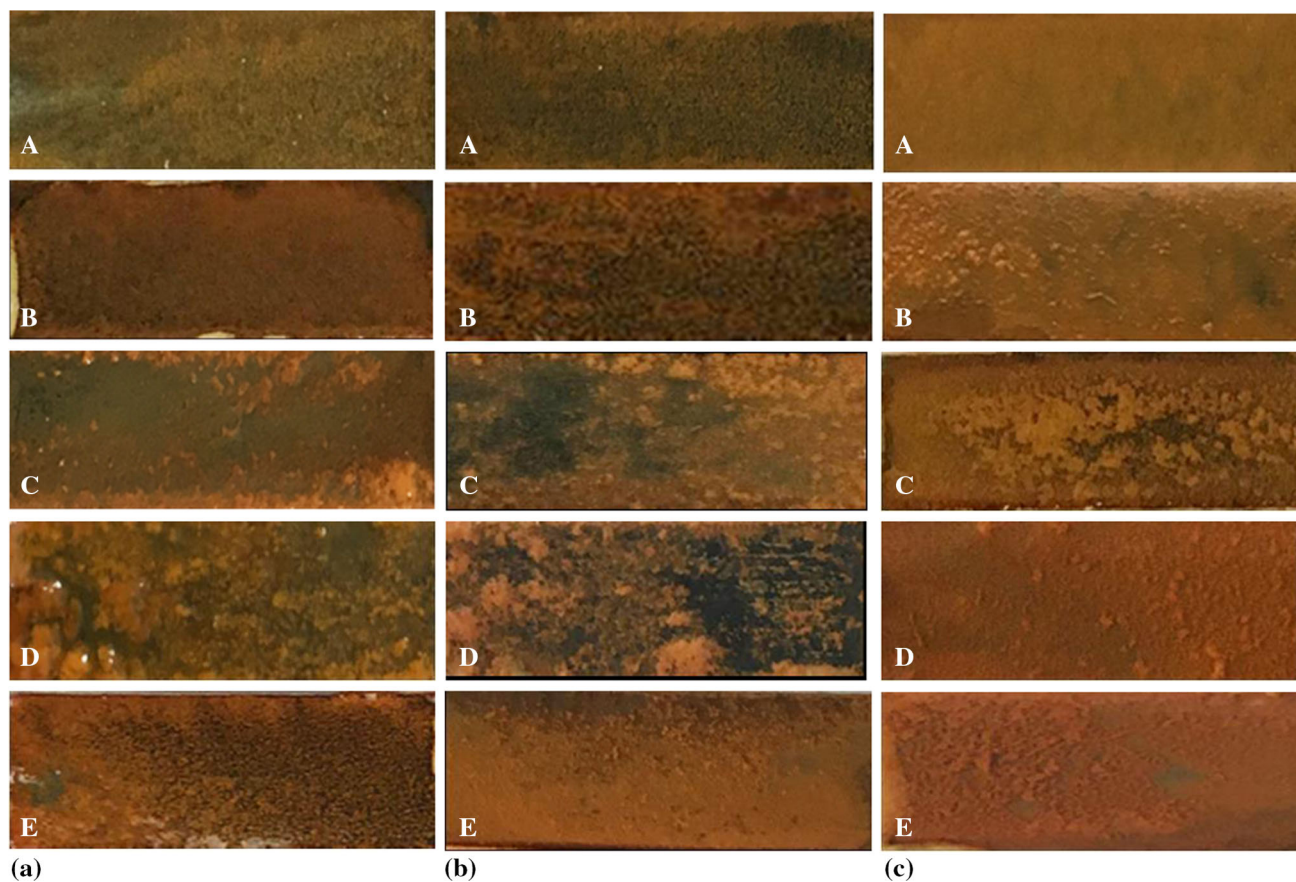
Fig. 9 The macro-morphology of X70 steel immersed in Dagang solution for 24 h under different AC densities. (a) X70 steel samples at different AC current densities (A) 0 A/m^2, (B) 30 A/m^2, (C) 100 A/m^2, (D) 200 A/m^2 and (E) 300 A/m^2. (b) X70 steel specimens with 150.9 MPa tensile stress at different AC current densities of the corrosion morphology (A) 0 A/m^2, (B) 30 A/m^2, (C) 100 A/m^2, (D) 200 A/m^2 and (E) 300 A/m^2. (c) X70 steel specimens with 150.9 MPa tensile stress and 30 A/m^2 DC interference at different AC current densities of the corrosion morphology (A) 0 A/m^2, (B) 30 A/m^2, (C) 100 A/m^2, (D) 200 A/m^2 and (E) 300 A/m^2

formation of corrosion pits, and the metal corroded in uniform corrosion. At the high AC density of 200-300 A/m^2, pitting corrosion occurs in X70 steel, and there are many punctured corrosion pits on the surface of X70 steel; some small pits would form larger pits together, and the distribution of large pits is relatively concentrated. Guo et al. (Ref 40) noticed that the X60 steel corrosion morphology under AC interference changed from uniform corrosion to pitting corrosion in a simulated soil solution.

Comparing the SEM images of X70 samples in Fig. 10(a) and (b), smaller external tensile stress (Ts = 150.9 MPa) would suppress pitting corrosion of X70 steel in alkaline soils, and the number and depth of pitting pits decrease. This is consistent with the conclusions of Wei et al. (Ref 41).

Comparing the SEM images of X70 samples in Fig. 10(b) and (c), when 150.9 MPa tensile stress and 30 A/m^2 DC interference are applied, it can be seen that the addition of DC promotes the uniform corrosion in the no AC interference or low AC current density ($\leq$ 30 A/m^2). Although pits were found on the sample surface under 200-300 A/m^2 AC interference, both pit amount and pit depth were not at the same level as that without tensile stress.

To sum up, it can be concluded that the stray AC would promote the local corrosion, while stray DC emphasizes more on uniform corrosion.

4. Conclusion

(1) AC interference negatively shifts the value of the OCP and the corrosion potential ($E_{corr,AC}$), which meaning that the metal tends to corrode. With the increase in AC density, the negative shift of corrosion potential increases. This phenomenon is well explained by the mathematical model of electrode polarization behavior from thermodynamics and kinetics.

(2) Comparing the corrosion rate calculated by weight loss method, it can be seen that the corrosion rate of X70 steel under the coupling of AC + Stress has little difference with the single AC, which shows that the stress has little effect on the corrosion resistance of X70 steel in the elastic phase. At the same AC density, the corrosion rate of X70 steel is about 5.8 times of that without direct current interference when 30 A/m^2 direct current interference is applied. The addition of DC greatly accelerates the corrosion of X70 steel, and the influence of DC stray on corrosion of pipeline steel is much greater than that of AC stray current on corrosion of pipeline steel. Therefore, the direct current has the greatest influence on corrosion of pipeline steel, followed by alternating current and finally stress.
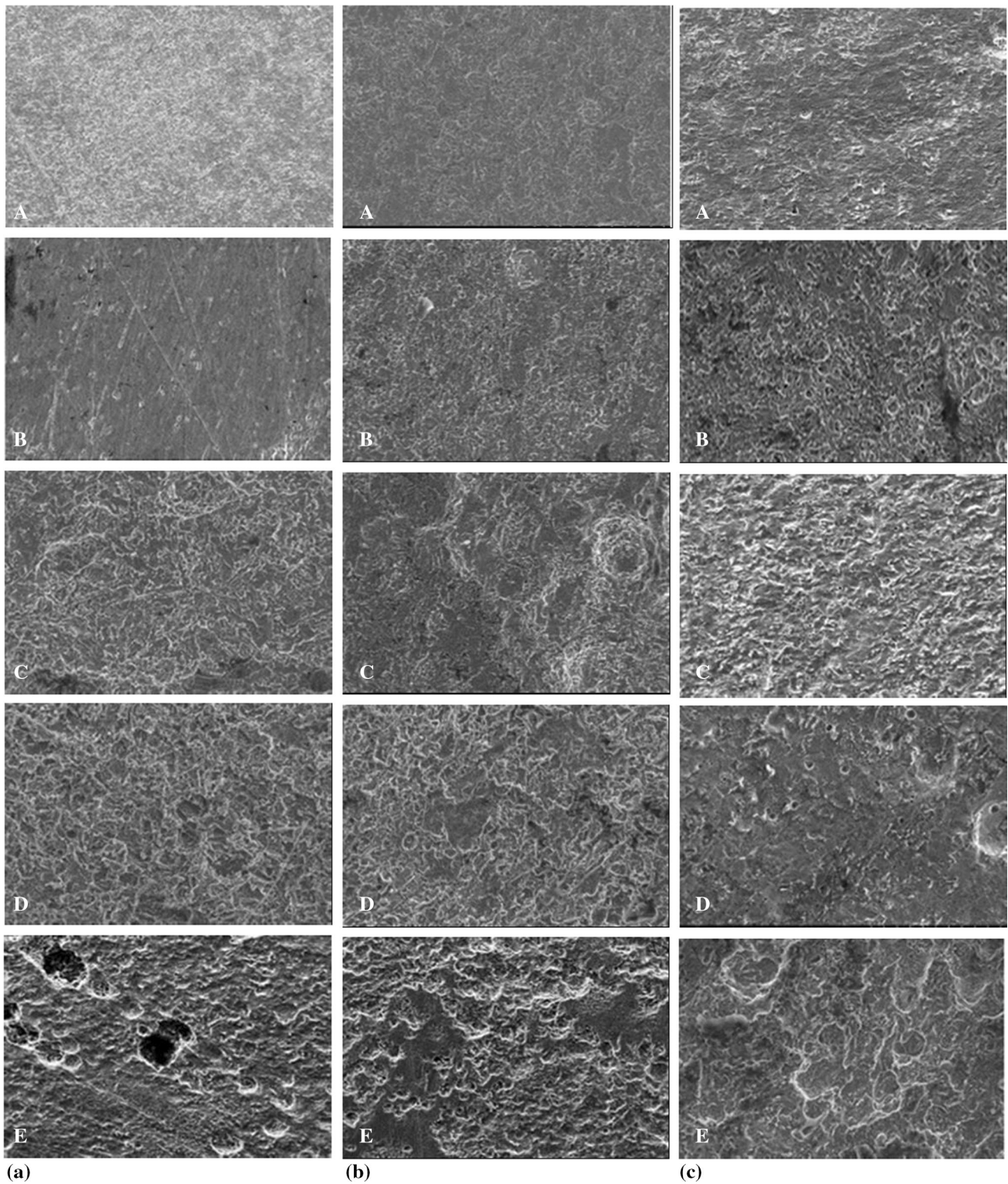
Fig. 10 SEM images of X70 samples with 150 MPa tensile stress at various stray AC densities in Dagang simulated soil solution. (a) Dagang simulated soil solution (A) 0 A/m^2, (B) 30 A/m^2, (C) 100 A/m^2, (D) 200 A/m^2 and (E) 300 A/m^2. (b) Dagang simulated soil solution with 150.9 MPa tensile stress (A) 0 A/m^2, (B) 30 A/m^2, (C) 100 A/m^2, (D) 200 A/m^2 and (E) 300 A/m^2. (c) Dagang simulated soil solution with a 150 MPa tensile stress and 30 A/m^2 DC interference (A) 0 A/m^2, (B) 30 A/m^2, (C) 100 A/m^2, (D) 200 A/m^2 and (E) 300 A/m^2

(3) No AC interference or low AC density interference (≤ 30 A/m^2) would result in uniform corrosion of X70 steel, and it will occur pitting corrosion with the alternating current density increase. Applying a small external tensile stress (Ts = 150.9 MPa) to X70 steel has a certain inhibitory effect on the occurrence of pitting corrosion. Applying DC interference, when no AC interference or low AC density interference (≤ 30 A/m^2) was

applied, would promote uniform corrosion, and high AC current density suppresses the occurrence of pitting corrosion.

References

1. S.R. Allahkaram, M. Isakhani-Zakaria, M. Derakhshani et al., Investigation on Corrosion Rate and a Novel Corrosion Criterion for Gas Pipelines Affected by Dynamic Stray Current, *J. Nat. Gas Sci. Eng.*, 2015, **26**, p 453–460
2. A.O.S. Solgaard, M. Carsana, M.R. Geiker et al., Experimental Observations of Stray Current Effects on Steel Fibres Embedded in Mortar, *Corros. Sci.*, 2013, **74**, p 1–12
3. Q. Zhu, A. Cao, Z. Wang et al., Stray Current Corrosion in Buried Pipeline, *Anti-Corros. Methods Mater.*, 2013, **58**(5), p 234–237
4. L. Bertolini, M. Carsana, and P. Pedeferri, Corrosion Behaviour of Steel in Concrete in the Presence of Stray Current, *Corros. Sci.*, 2007, **49**(3), p 1056–1068
5. T.J. Barlo and A.D. Zdunek, *Stray Current Corrosion in Electrified Rail System-Final Report*. (Infrastructure Technology Institute, Evanston Illinois, 1995), pp. 1–47
6. Z.G. Chen, C.K. Qin, J.X. Tang et al., Experiment Research of Dynamic Stray Current Interference on Buried Gas Pipeline from Urban Rail Transit, *J. Nat. Gas Sci. Eng.*, 2013, **15**(6), p 76–81
7. H.R. Hanson, AC Corrosion on a Pipeline Located in an HVAC Utility Corridor, in *Corrosion* (2004)
8. M. Ouadah, O. Touhami, R. Ibtiouen et al., Corrosive Effects of the Electromagnetic Induction Caused by the High Voltage Power Lines on Buried X70 Steel Pipelines, *Int. J. Electr. Power Energy Syst.*, 2017, **91**, p 34–41
9. X.H. Wang, J.Y. Liu, H.E. Ren-Yang et al., Detection Method of Stray Current to Urban Buried Gas Pipelines, in *Pipeline Technique & Equipment* (2010)
10. S.Y. Xu, W. Li, and Y.Q. Wang, Effects of Vehicle Running Mode on Rail Potential and Stray Current in DC Mass Transit Systems, *IEEE Trans. Veh. Technol.*, 2013, **62**(8), p 3569–3580
11. Z.X. Tang, Z.J. Wen, C.S. Li et al., Corrosion Behavior of Carbon Steel in Interference of Stray Current and Cathodic Protection, *Surf. Technol.*, 2015, **44**(12), p 12–18
12. M. Ouadah, O. Touhami, R. Ibtiouen et al., Method for Diagnosis of the Effect of AC on the X70 Pipeline Due to an Inductive Coupling Caused by HVPL, *IET Sci. Meas. Technol.*, 2017, **11**(6), p 766–772
13. Y. Li, Effects of Stray AC Interference on Corrosion Behavior of X70 Pipeline Steel in a Simulated Marine Soil SolutionJ], *Int. J. Electrochem. Sci.*, 2017, **12**(3), p 1829–1845
14. Z. Jiang, Y. Du, M. Lu et al., New Findings on the Factors Accelerating AC Corrosion of Buried Pipeline, *Corros. Sci.*, 2014, **81**(81), p 1–10
15. B. Mccollum and G.H. Ahlborn, The Influence of Frequency of Alternating or Infrequently Reversed Current on Electrolytic Corrosion, *Proc. Am. Inst. Electr. Eng.*, 2013, **35**(3), p 371–397
16. S. Goidanich, L. Lazzari, and M. Ormellese, AC Corrosion. Part 2: Parameters Influencing Corrosion Rate, *Corros. Sci.*, 2010, **52**(3), p 916–922
17. X. Wang and X. Wang, Effects of Stray AC on Delamination of Epoxy Coatings with Defects in 3.5% NaCl Solution, *Int. J. Electrochem. Sci.*, 2017, **12**(7), p 6520–6534
18. X. Wang, X. Tang, L. Wang et al., Corrosion Behavior of X80 Pipeline Steel under Coupling Effect of Stress and Stray Current, *Int. J. Electrochem. Sci.*, 2014, **9**(8), p 4574–4588
19. Y. Chen, Cathodic Protection Parameters of X65 and X80 Pipeline Steels in Dagang Simulated Soil Solution, *Surf. Technol.*, 2018, **47**(6), p 218–223
20. Z. Liu, Z. Cui, X. Li et al., Mechanistic Aspect of Stress Corrosion Cracking of X80 Pipeline Steel Under Non-Stable Cathodic Polarization, *Electrochem. Commun.*, 2014, **48**, p 127–129
21. N. Winzer, A. Atrens, G. Song et al., A Critical Review of the Stress Corrosion Cracking (SCC) of Magnesium Alloys, *Adv. Eng. Mater.*, 2010, **7**(8), p 659–693
22. Z.Y. Liu, X.G. Li, and Y.F. Cheng, Mechanistic Aspect of Near-Neutral pH Stress Corrosion Cracking of Pipelines Under Cathodic Polarization, *Corros. Sci.*, 2012, **55**(2), p 54–60
23. G.V. Boven, R. Rogge, and W. Chen, Residual Stress and Stress Corrosion Cracking of High Pressure Hydrocarbon Transmission Pipelines, in *International Pipeline Conference* (2007), pp. 725–742
24. Y. Wei, H. Feng, H.U. Qian et al., Influences of Applied Tensile Stress on the Pitting Electrochemical Behavior of X80 Pipeline Steel, *J. Chin. Soc. Corros. Protect.*, 2013, **33**(4), p 277–282
25. Z.Y. Liu, X.G. Li, and Y.F. Cheng, Electrochemical State Conversion Model for Occurrence of Pitting Corrosion on a Cathodically Polarized Carbon Steel in a Near-Neutral pH Solution, *Electrochim. Acta*, 2011, **56**(11), p 4167–4175
26. M. Büchler, Alternating Current Corrosion of Cathodically Protected Pipelines: Discussion of the Involved Processes and Their Consequences on the Critical Interference Values, *Mater. Corros.*, 2015, **63**(12), p 1181–1187
27. M. Büchler, T. Watari, and W.H. Smyrl, Investigation of the Initiation of Localized Corrosion on Aluminum Alloys by Using Fluorescence Microscopy, *Corros. Sci.*, 2000, **42**(9), p 1661–1668
28. L.Y. Xu and Y.F. Cheng, An Experimental Investigation of Corrosion of X100 Pipeline Steel Under Uniaxial Elastic Stress in a Near-Neutral pH Solution, *Corros. Sci.*, 2012, **59**(3), p 103–109
29. L. Yang, N. Hort, R. Willumeit et al., Effects of Corrosion Environment and Proteins on Magnesium Corrosion, *Br. Corros. J.*, 2014, **47**(5), p 335–339
30. X.U. Chun-chun and L. Chi, Electrochemical Behavior of X70 Pipeline Steel in Carbonate-Bicarbonate Solution, *Corros. Sci. Protect. Technol.*, 2004, **16**(5), p 268–271
31. F. Mansfeld, Tafel Slopes and Corrosion Rates Obtained in the pre-Tafel Region of Polarization Curves, *Corros. Sci.*, 2005, **47**(12), p 3178–3186
32. U. Bertocci, AC Induced Corrosion. The Effect of an Alternating Voltage on Electrodes Under Charge-Transfer Control, *Corrosion*, 1979, **35:5**(5), p 1281–1287
33. L. Liang, Y. He, H. Song et al., Effect of Hydration Pretreatment on Tunnel Etching Behaviour of Aluminium Foil, *Corros. Sci.*, 2013, **70**(3), p 180–187
34. Y. Guo, T. Meng, D. Wang et al., Experimental Research on the Corrosion of X Series Pipeline Steels Under Alternating Current Interference, *Eng. Fail. Anal.*, 2017, **78**, p 87–98
35. S.B. Lalvani and X.A. Lin, A Theoretical Approach for Predicting AC-Induced Corrosion, *Corros. Sci.*, 1994, **36**(6), p 1039–1046
36. X. Wang, X. Tang, L. Wang et al., Corrosion Behavior of X80 Pipeline Steel under Coupling Effect of Stress and Stray Current, *Int. J. Electrochem. Sci.*, 2014, **9**(8), p 4574–4588
37. C. Wen, J. Li, S. Wang et al., Experimental Study on Stray Current Corrosion of Coated Pipeline Steel, *J. Nat. Gas Sci. Eng.*, 2015, **27**, p 1555–1561
38. M. Büchler and H.-G. Schöneich, Investigation of Alternating Current Corrosion of Cathodically Protected Pipelines: Development of a Detection Method, Mitigation Measures, and a Model for the Mechanism, *Corrosion*, 2012, **65**(9), p 578–586
39. Z. Tang, S. Hong, W. Xiao et al., Characteristics of Iron Corrosion Scales Established Under Blending of Ground, Surface, Saline Waters and Their Impacts on Iron Release in the Pipe Distribution System, *Corros. Sci.*, 2006, **48**(2), p 322–342
40. Y.B. Guo, C. Liu, D.G. Wang et al., Effects of Alternating Current Interference on Corrosion of X60 Pipeline Steel, *Petrol. Sci.*, 2015, **12**(2), p 316–324
41. Y. Wei, H. Feng, H.U. Qian et al., Influences of Applied Tensile Stress on the Pitting Electrochemical Behavior of X80 Pipeline Steel, *J. Chin. Soc. Corros. Protect.*, 2013, **33**(4), p 277–282

Publisher's Note Springer Nature remains neutral with regard to jurisdictional claims in published maps and institutional affiliations.